

Trajectory Optimization under Contact Timing Uncertainties

Haizhou Zhao¹, Majid Khadiv¹

Abstract—Most interesting problems in robotics (e.g., locomotion and manipulation) are realized through intermittent contact with the environment. Due to the perception and modeling errors, assuming an exact time for establishing contact with the environment is unrealistic. On the other hand, handling uncertainties in contact timing is notoriously difficult as it gives rise to either handling uncertain complementarity systems or solving combinatorial optimization problems at run-time. This work presents a novel optimal control formulation to find robust control policies under contact timing uncertainties. Our main novelty lies in casting the stochastic problem to a deterministic optimization over the uncertainty set that ensures robustness criterion satisfaction of candidate pre-contact states and optimizes for contact-relevant objectives. This way, we only need to solve a manageable standard nonlinear programming problem without complementarity constraints or combinatorial explosion. Our simulation results on multiple simplified locomotion and manipulation tasks demonstrate the robustness of our uncertainty-aware formulation compared to the nominal optimal control formulation.

I. INTRODUCTION

Intermittent contact with the world renders locomotion and object manipulation problems hybrid. When using optimal control to generate plans for these systems, the resulting problem to solve would be a mixed-integer optimization problem [1], [2]. Several works have tried to solve the problem by relaxing the hybrid nature, e.g., smoothing the contact transition by regularizing the Delassus matrix [3], handling physical consistency as a soft constraint [4], or relaxing contact with complementarity slackness in the solver [5]. Most recent efforts to implement MPC for locomotion and manipulation have focused on solving a hierarchical problem instead of the holistic one and could achieve impressive behaviors on real hardware [6], [7], [8], [9], [10]. These approaches consider a fixed contact plan and control the whole body motion for the given plan. They also assume that contact events happen at exact times, i. e., the predefined switching times. However, in reality, this is a very restrictive assumption. For instance, the robot’s perception of the environment is always with some errors. Furthermore, the tracking error of the end-effector establishing contact can also lead to a mismatch between the planned and realized time of contact. To handle these situations, the whole-body MPC frameworks available in the literature either use heuristics [8] or rely on the intrinsic robustness of MPC through fast replanning to handle uncertainties in contact events [6], [9], [7]. However, these approaches are very limited and a more systematic approach is required.

¹Munich Institute of Robotics and Machine Intelligence, Technical University of Munich, Germany haizhou.zhao@outlook.com, majid.khadiv@tum.de

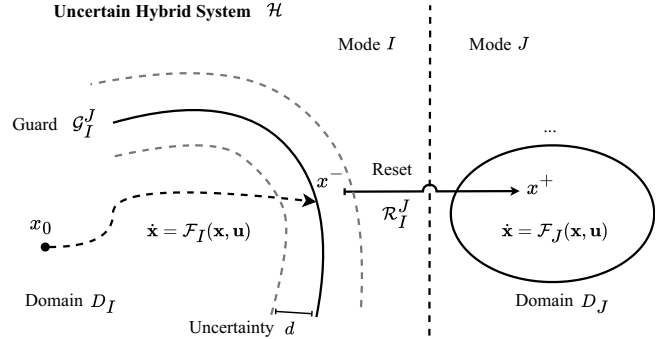


Fig. 1. Illustration of Uncertain Hybrid Systems

Recently, [11], [12], [13], [14] investigated the use of robust and stochastic optimal control for contact-rich robotics problems. While these approaches provide a very concrete understanding of the problem and interesting safety guarantees, they generally fall short in handling contact timing uncertainty. [12] has shown that adjusting the end-effector impedance as a function of disturbances can mitigate the problem of impact when the contact event is uncertain. In this framework, the contact event is considered to be uncertain with a known distribution, and the impact is mitigated using a risk-sensitive optimal controller. However, not adapting desired trajectories can highly limit the capability of the controller in handling different situations such as late foot touch-down during locomotion.

The primary contribution of this work is to provide a deterministic re-formulation of the stochastic hybrid optimal control problem with uncertainty in the switching event that does not add run-time computational complexity compared to the deterministic optimal control problem. In doing so, we propose a robust optimal control formulation that accounts for a trajectory of possible switching states over the uncertainty set. The proposed approach can be adapted for general contact dynamics from locomotion to manipulation. Through several simplified examples on locomotion and manipulation problems, we demonstrate the robustness of our approach compared to the standard nominal optimal control problem.

The rest of the paper is structured as follows: in Section II, we provide the necessary ingredients to formulate the problem. In section III, we detail our proposed formulation. In section IV, we present the results of applying our formulation to several simplified locomotion and manipulation problems. Finally, Section V presents the concluding remarks

and future work.

II. PRELIMINARIES

In this section, we first define the terminology required for describing our problem. Then, we present a deterministic optimal control formulation for hybrid dynamical systems.

A. Deterministic Hybrid Systems

Locomotion and manipulation are realized through intermittent contact with the environment. One way to formalize this problem is through the framework of hybrid dynamical systems [15]. In this work, we consider the following definition of hybrid systems [16], [17]

$$\mathcal{H} : \begin{cases} \dot{\mathbf{x}} = \mathcal{F}_I(\mathbf{x}, \mathbf{u}), & \mathbf{x} \in \mathcal{D}_I \setminus \mathcal{G}_I^J, \mathbf{u} \in \mathcal{U}_I, \\ \mathbf{x}^+ = \mathcal{R}_I^J(\mathbf{x}^-), & \mathbf{x}^- \in \mathcal{G}_I^J, \mathbf{x}^+ \in \mathcal{D}_J, \end{cases} \quad (1)$$

with $\mathcal{J} = \{I, J, \dots\}$ being the finite set of discrete modes such that for a mode $I \in \mathcal{J}$,

- \mathcal{F}_I is the continuous dynamics,
- \mathcal{D}_I is the domain of states,
- \mathcal{U}_I is the set of admissible input,
- $\mathcal{G}_I^J := \{\mathbf{x} \in \mathcal{D}_I | g_I^J(\mathbf{x}) \leq 0\}$ is the guard (Fig. 1),
- $\mathcal{R}_I^J : \mathcal{G}_I^J \rightarrow \mathcal{D}_J$ is the reset map that projects states in \mathcal{D}_I to \mathcal{D}_J when the guard condition $g_I^J(\mathbf{x}^-) \leq 0$ is met.

A simple example of a hybrid robotic system is a jumping 1D hopper. Upon landing, the robot's states enter the guard from the aerial phase to stance, undergoing a reset by an impulsive impact force.

B. From Hybrid to Switching systems

Given the sequence of contacts for a hybrid system, the problem can be simplified to a switching system. In this formulation, the system's dynamics are smooth between consecutive switches, while the time of the switch can still be optimized. Recently, many fast solvers [18], [19], [20] have been developed for real-time resolution of (2). In the following, we present the multiple-shooting transcription of the switching system.

Let \mathcal{S} be the set of shooting node indices where a switch is expected. For a given initial state \mathbf{x}_0 , the time-based direct-multiple-shooting optimal control problem can be formulated as

$$\min_{\mathbf{x}, \mathbf{u}} L_N(\mathbf{x}_N) + \sum_{i=0}^{N-1} L_i(\mathbf{x}_i, \mathbf{u}_i) \quad (2a)$$

$$\text{s.t. } \forall i \notin \mathcal{S} : \quad \mathbf{f}_i(\mathbf{x}_i, \mathbf{u}_i, \mathbf{x}_{i+1}, \Delta t_i) = \mathbf{0}, \quad (2b)$$

$$g_i(\mathbf{x}_{i+1}) > 0, \quad (2c)$$

$$\forall i \in \mathcal{S} : \quad \mathbf{f}_i(\mathbf{x}_i, \mathbf{u}_i, \mathbf{x}_{i+1}^-, \Delta t_i) = \mathbf{0}, \quad (2d)$$

$$\mathbf{x}_{i+1} = \mathcal{R}_i(\mathbf{x}_{i+1}^-), \quad (2e)$$

$$g_i(\mathbf{x}_{i+1}^-) = 0, \quad (2f)$$

$$\mathbf{h}(\mathbf{x}_i, \mathbf{u}_i) \leq 0, \quad (2g)$$

where Δt_i is the phase-wise timestep, N is the number of shooting nodes, L_N is the terminal cost, L_i is the running cost, (2b) is the non-switching implicit dynamics, (2d) is the pre-switching continuous dynamics derived from $\mathcal{F}_{(\cdot)}$ in (1), \mathbf{x}_{i+1}^- denotes the pre-reset state, (2c),(2f) ensure switching consistency, (2e) is the state reset equation at the switch, and (2g) is the state-input inequality constraints.

III. UNCERTAINTY-AWARE OPTIMAL CONTROL

The formulation in (2) assumes that contact happens at a certain time and state (where the distance between the end-effector and the environment goes to zero). However, due to uncertainties in the environment perception and end-effector tracking errors, it is highly unlikely that the end-effector touches the ground at the exact pre-defined time. To formalize this situation, we introduce the following uncertain guard as illustrated in Fig. 1:

$$\hat{\mathcal{G}}_I^J(\delta) = \{\mathbf{x} \in \mathcal{D}_I | g_I^J(\mathbf{x}) \leq \delta\}, \delta \in [-d, d], \quad (3)$$

where δ is the guard uncertainty bounded by d . With $\hat{\mathcal{G}}$, a state cannot be deterministically predicted to incur switching, leading to uncertain contact timing and thus the switching time between modes. This is naturally incompatible with the deterministic structure of (2).

A. Issues of the Nominal Approach

Trajectories generated from nominal time-based optimal control with a nominal guard ($\delta = 0$) only ensure that the nominal switching state is feasible. If the switching does not happen as planned (i.e., early or late contact), the system may evolve unexpectedly. Typical issues include:

- For late contact, the controller is unknown after the nominal contact timing. Problem-specific solutions include reference spreading [21] or simplistic zero-order-hold of the last input.
- For early contact, the system usually encounters unfavorable impact forces. In such cases, the system may fail due to failures in the mechanical structure or bouncing of the end-effector impacting the ground.
- Since the nominal problem is only concerned with the exact contact event, it can lead to highly aggressive motions before or after contact. An example is that when a trajectory is aggressive for performance, states near its nominal switching time may be outside the feasibility set of the post-impact problem.

In this section, we introduce our main contribution: an uncertainty-aware optimal control formulation that resolves the above issues.

B. A Deterministic Transcription

Intuitively, a robust time-based trajectory that solves the problem in Sec. III-A should be deterministic until a switch is triggered. Since the switching may happen at any moment, when the states are within the uncertain region, all these candidate pre-switching states should not harm the system safety or the feasibility of the post-switch optimal control. Based on this intuition, we consider that for a single phase, an

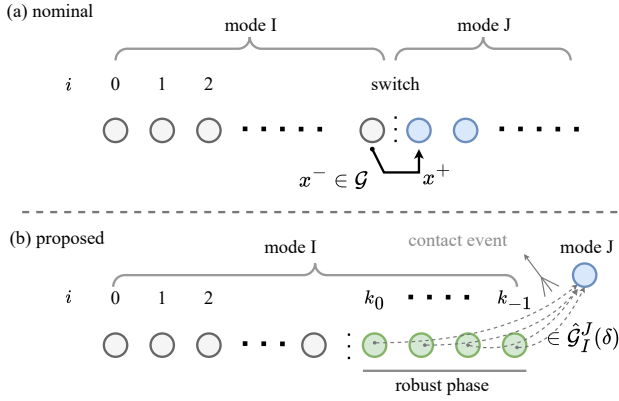


Fig. 2. Illustration of the difference between (a) the nominal optimal control and (b) the proposed approach. The proposed method does not switch the mode but generates a trajectory of feasible switching states over the uncertainty set.

uncertain sub-phase (namely the *robust phase*) is appended to the pre-switching phase. For its index set \mathcal{K} , the following constraints must be satisfied:

$$i = \mathcal{K}_0, g_i(\mathbf{x}_i) = d, \quad (4a)$$

$$i = \mathcal{K}_{-1}, g_i(\mathbf{x}_i) = -d, \quad (4b)$$

$$\forall i \in \mathcal{K}, \dot{g}_i(\mathbf{x}_i) \leq 0, \quad (4c)$$

where $\mathcal{K}_0, \mathcal{K}_{-1}$ denote the earliest and latest indices in \mathcal{K} , respectively. An uncertainty-aware optimal control problem can then be formulated as a parameterized optimization problem as introduced in [22]:

$$\min_{\mathbf{x}, \mathbf{u}, \Delta t, d} \sum_{i=0}^{N-1} L_i(\mathbf{x}_i, \mathbf{u}_i) + \sum_{i \in \mathcal{K}} L_K(\mathbf{x}_i, \mathbf{p}_i) \quad (5a)$$

$$\text{s.t. } \mathbf{h}_K(\mathbf{x}_i, \mathbf{p}_i) \leq \mathbf{0}, \forall i \in \mathcal{K}, \quad (5b)$$

$$\Delta t_i \in [\Delta t_{\min}, \Delta t_{\max}], d \in [d_{\min}, d_{\max}], \quad (5c)$$

$$\forall i \notin \mathcal{K}, (2c),$$

$$\forall i \in \mathcal{K}, (4),$$

$$(2b), (2g)$$

where $\mathcal{K}_0 = N$, L_K is the contact-related objective, \mathbf{h}_K is the contact-related constraint, and \mathbf{p}_i is the collection of auxiliary variables including the timesteps and uncertainty. Notice that δt and d are decision variables in this new formulation, bounded by (5c), which can be crucial for the feasibility and convergence of the optimization problem. For instance, depending on the problem if d is set to a large fixed value, there might be no feasible solution that can satisfy all the constraints for all the possible contact events. Also, since the number of nodes in the robust phase is fixed, optimizing time is important to regulate the robot's behavior in the uncertain region.

The *robust phase* in (4) ensures that the trajectory traverses the uncertain region, constituting a continuous collection of possible switching states. To show the effectiveness of our proposed formulation in (5) in generating robust trajectories, we can adapt L_K, \mathbf{h}_K in (5b) in the following ways: we

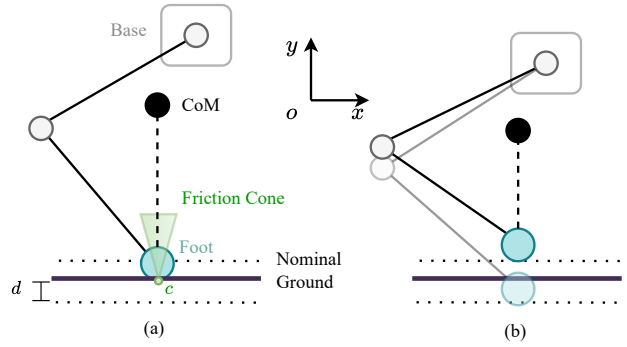


Fig. 3. Illustration of the planar two-link point-footed robot. (a) The robot has two joints (hip and knee) and a 2-DoF base joint. The black dot denotes the whole-body center of mass (CoM). (b) When landing, the ground position is uncertain.

can model safety-related or feasibility-related criteria as inequality constraints \mathbf{h}_K ; we can also adapt L_K to reach various goals such as robustness maximization and impact minimization. We will show the flexibility of our formulation in different case studies in the next section.

Remark 1 (Uncertainty optimization) In (5), uncertainty d is also a decision variable. Depending on the specific problem setting, this handling enables finding the maximum possible uncertainty, where either the uncertainty can be increased to gain better robustness or decreased to show the maximum feasible value.

Remark 2 (Optimality) For long-term optimality, the formulation in (5) can further be extended to a parallelizable tree-structured optimal control problem [23] that branches at each shooting node in \mathcal{K} . Nevertheless, we only focus in this paper on the transcription of the uncertainty into a robust phase without trying to achieve long-term optimality.

IV. CASE STUDIES

In this section, we show case studies of various locomotion and manipulation tasks based on the proposed optimal control formulation. We also compare the results of our proposed robust formulation to the nominal case. All examples are implemented using the Opti stack of CasADi [24] and IPOPT [25].

A. Impact Minimization of a Hopping Robot

One of the classical examples in robot locomotion control is impact minimization for jumping robots [26]. In this task, a planar two-link point-foot hopper jumps continuously while the height of the support surface can suddenly change within a bound, as shown in Fig. 3. The robot has a 2-DoF X-Y base joint. The task is to perform in-place hopping to reach a desired height.

1) *Dynamic Model*: Let $\mathbf{q} = [y_b, \theta_h, \theta_k]^T$, and $\dot{\mathbf{q}} = [\dot{y}_b, \dot{\theta}_h, \dot{\theta}_k]^T$. y_b is the base height, and θ_h, θ_k are the hip and knee angles, respectively. The dynamics of the system can be written as

$$\mathbf{M}(\mathbf{q})\ddot{\mathbf{q}} + \mathbf{H}(\mathbf{q}, \dot{\mathbf{q}}) = \mathbf{S}\boldsymbol{\tau} + \mathbf{J}_c^T \mathbf{F}_c, \quad (6a)$$

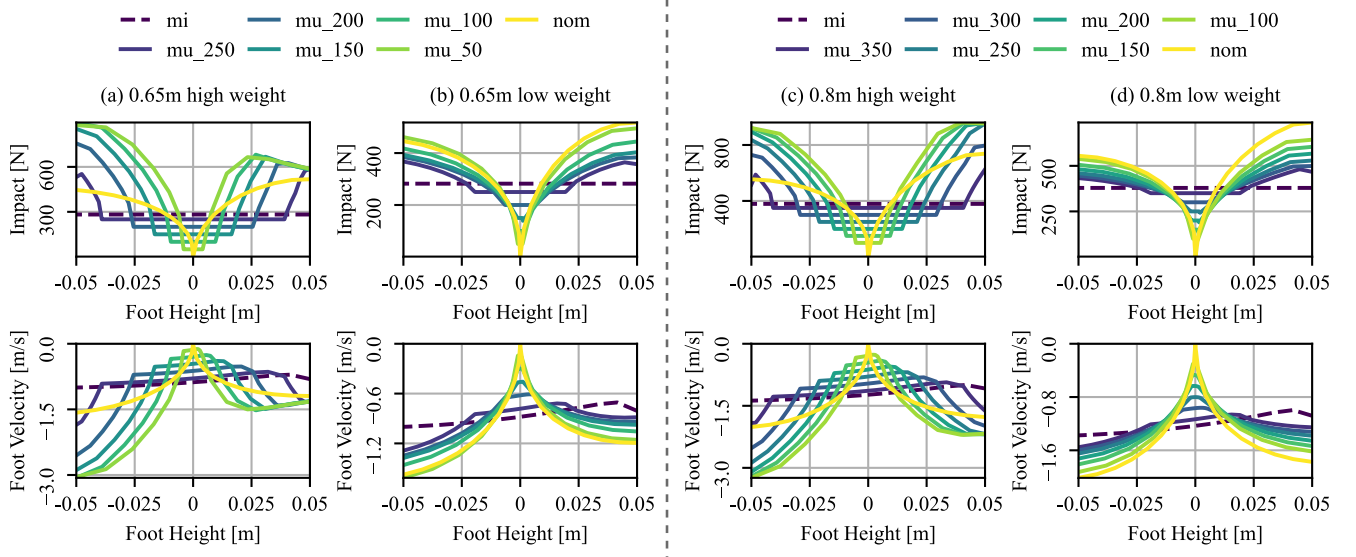


Fig. 4. Simulation data during the robust phase. The weights for maximizing the uncertainty in (a),(c) are respectively 1000x that in (b),(d). 'mi' denotes the impact minimization over the given uncertainty $[-0.05, 0.05]$ m. 'mu_(x)' denotes uncertainty maximization for known impact limits x (unit: N), where the flat region denotes the uncertainty. 'nom' denotes the nominal optimal control data. Flat parts of 'mu_(x)' denote the optimized uncertainty region where the impact limits are satisfied.

where $\mathbf{M} \in \mathbb{R}^{3 \times 3}$ is the joint-space inertia matrix, $\mathbf{H} \in \mathbb{R}^3$ is the nonlinear effects, $\mathbf{S} = [\mathbf{0}_{2 \times 2} \quad \mathbf{I}_2]^\top$ is the selection matrix, $\boldsymbol{\tau} \in \mathbb{R}^2$ is the joint torques, $\mathbf{J}_c \in \mathbb{R}^{2 \times 3}$ is the foot contact jacobian, $\mathbf{F}_c = [F_y, F_x]^\top \in \mathbb{R}^2$ is the contact force subject to the following constraints:

$$0 < F_y \perp y_f - y_g > 0, \quad (7a)$$

$$F_y \geq \mu |F_x|, \quad (7b)$$

where (7a) is the contact complementary constraints, y_f, y_g are the foot and the ground height, respectively. Equation (7b) encodes the planar friction cone constraint. We assume purely inelastic impact, i.e., zero post-impact foot velocity. Based on maximum dissipation principle, the impact impulse $\boldsymbol{\lambda} = [\lambda_x, \lambda_y]^\top$ can be modeled as

$$\boldsymbol{\lambda} = \arg \min \|\mathbf{J}_c^T \dot{\mathbf{q}}^+\|^2 \quad (8a)$$

$$\text{s.t. } \mathbf{M}(\dot{\mathbf{q}}^+ - \dot{\mathbf{q}}^-) = \mathbf{J}_c^T \boldsymbol{\lambda} + [\mathbf{S}\boldsymbol{\tau} - \mathbf{H}(q, \dot{\mathbf{q}}^-)]\Delta t, \quad (8b)$$

$$\lambda_y \geq \mu |\lambda_x|, \quad (8c)$$

$$\mathbf{J}_c^N \dot{\mathbf{q}}^+ = 0, \quad (8d)$$

where the superscription N and T denote normal and tangential components of velocity w.r.t. the ground, Δt denotes the impact duration, which is set to be 2ms in our tests. Note that impulse is used instead of force to improve the numerical conditioning.

2) *Nominal Optimal Control*: In the form of (2), a hopping loop is divided into three phases: take-off (stance), ascendance, and falling. A terminal constraint of the base height is added to the ascendance phase to ensure the base reaches the desired position. The guard is chosen as

$$g_i := y_f - y_g. \quad (9)$$

Let $\mathbf{r}_f = [x_f, y_f]^\top$. To maintain the discretized contact constraint during the stance phase, we add the velocity-level

stabilization at each shooting node:

$$k_f \dot{\mathbf{r}}_f + \mathbf{r}_f = \mathbf{r}_f^0, \quad (10)$$

where $k_f = 1e3$ in our setting, \mathbf{r}_f^0 is the initial foot position. The center-of-mass (CoM) of the robot is set to be right above the foot during the whole procedure for in-place hopping. Upon switching, (8) is added and the horizontal post-impact velocity of the foot is constrained to be zero as a terminal constraint of the falling phase to avoid slip. Torques, joint positions, and velocities are also constrained according to the hardware implementation of the robot for realistic settings.

3) *Robust Formulation*: The robust formulation is the same as the nominal one except that an extra robust phase is added. The guard (9) is used in the form of (4). Two realistic scenarios are tested to show the flexibility of our method:

- Minimizing impact force for the worst-case uncertainty within a given range. In this case, we minimize the upper bound of vertical impact $\bar{\lambda}_y$ in the robust phase, i.e.,

$$L_K := w_\lambda \bar{\lambda}_y, \quad (11a)$$

$$h_K := \lambda_y < \bar{\lambda}_y. \quad (11b)$$

Note that d is a parameter and $\bar{\lambda}_y$ is a decision variable.

- Maximizing uncertainty based on the worst-feasible impact force. This is the safety-critical case when the maximum tolerable impact by the structure of the robot $\bar{\lambda}_y$ is obtained from mechanical design. In this case, for the robust phase, we have:

$$L_K := -w_d d, \quad (12a)$$

$$h_K := \lambda_y < \bar{\lambda}_y. \quad (12b)$$

Note that $\bar{\lambda}_y$ is a parameter and d is a decision variable.

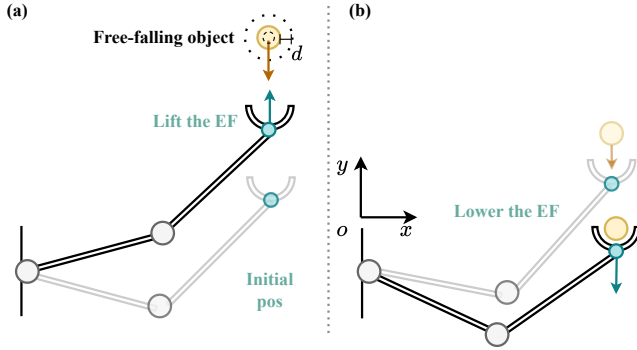


Fig. 5. Illustration of how the manipulator catches a free-falling object. The manipulator (a) lifts its end-effector (EF) to a high position and then (b) lowers its EF to reduce the velocity w.r.t. the object.

4) *Result and Discussion*: Two desired heights (0.65m, 0.8m) are tested for the nominal approach and the two scenarios of the robust approach. The friction coefficient is set at 0.7. The data is shown in Fig. 4. In terms of impact minimization, it can be observed that the robust method can have approximately up to 30%-50% improvement over the nominal method for about 70% of the uncertain region.

For uncertainty maximization, a wide range for the weight w_d is considered to generate diverse solutions. For low w_d , as the impact limit $\bar{\lambda} \rightarrow 0$, the robust solution converges to the nominal case. For high w_d , the feasible uncertainty can be larger, at the cost of higher impact force outside the uncertain region. The low w_d cases can also be interpreted as reducing the uncertainty to obtain better average improvements over the nominal method i.e., the percentage of the original uncertain region with lower impact forces than the nominal solution.

B. Object Catching

This task shows a torque-controlled manipulator catching an object, of which the shape is uncertain. It is a typical safety-critical case as an object can be fragile and may break if the impact upon contact is high. The setup is shown in Fig. 5. For simplicity, instead of using impulse as safety criteria, it is assumed that the object will crack if the impact velocity difference between the EF and the object exceeds a maximal value.

Let $y_{\text{object}}, y_{\text{EF}}$ be respectively the y-position of the nominal bottom of the object and the EF. The uncertain guard in (4) is chosen as

$$g_i := y_{\text{obj}} - y_{\text{EF}}, \quad (13)$$

with the following constraints on their x-positions to ensure consistent geometry during catching

$$\forall i \in \mathcal{K}, x_{\text{EF}} = x_{\text{obj}}, \dot{x}_{\text{EF}} = 0. \quad (14)$$

The initial state of the manipulator is set the same for all tests. The shoulder joint (the first joint attached to the fixed base) is located at the origin. The object falls from $y_{\text{obj}} = 1\text{m}$ and different x_{obj} . The results are shown in Fig. 6 for the following optimizer initializations:

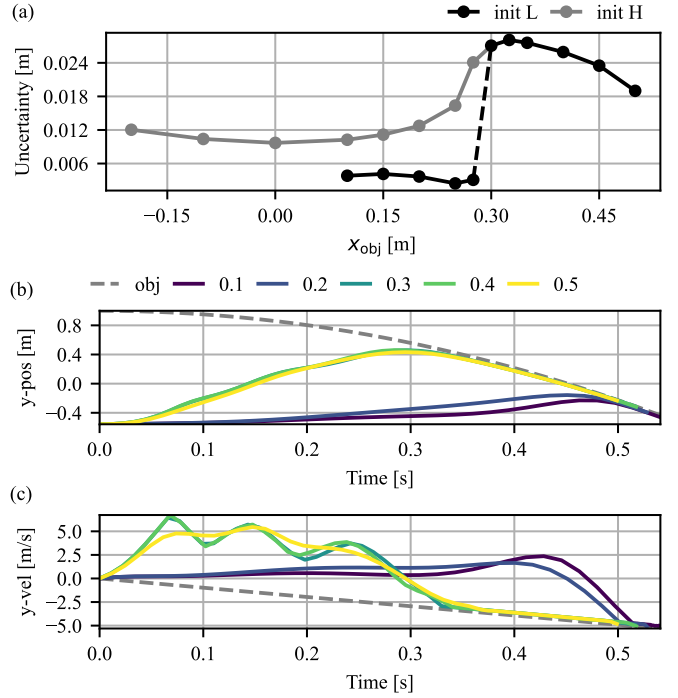


Fig. 6. Optimization and simulation data of the manipulator object-catching task. (a) The (solved) optimized uncertainty w.r.t. the initial x_{obj} with differential initializations. (b),(c) are the y-position and -velocity trajectories of the object and the EF with the 'init L' initialization, where the number denotes the x_{obj} . The manipulator follows the strategy of reducing velocity difference at possible impacts.

- 'init L': initialization using the initial state where $y_{\text{EF}} < 0$, i.e., the EF is lower than the shoulder joint.
- 'init H': initialization using the state where $y_{\text{EF}} > 0$, i.e., the EF is higher than the shoulder joint.

which lead to distinct optimized uncertainty as in Fig. 6(a). Optimization with 'init L' is infeasible with low x_{obj} . Solutions to the two initializations diverge from each other for $x_{\text{obj}} \approx 0.28$ as represented by the discontinuity (black dashed line). The y-position and velocity plots can further illustrate it as in Fig. 5(b,c) where for 'init L', the trajectories with $x_{\text{obj}} \in \{0.1, 0.2\}$ are different from the ones with $x_{\text{obj}} \in \{0.3, 0.4, 0.5\}$. This indicates that the uncertainty optimization is affected by the non-convexity of the original problem. As can be seen in 5(b,c), the manipulator reduces the velocity difference between its end-effector and the object to reduce the impact force.

C. Cart-Pole With a Rigid Wall

In this case, we test a task similar to [27] where a cart-pole system can use contact with the wall to stabilize itself under disturbance. As shown in Fig. 7, the pole will bounce when colliding with a rigid wall, and the cart position is limited.

1) *Dynamic Model*: Let $\mathbf{q} = [x, \theta]$ where x is the cart position and θ is the counterclockwise pole angle. Similar to the hopping robot, the equation of motion of the cart-pole

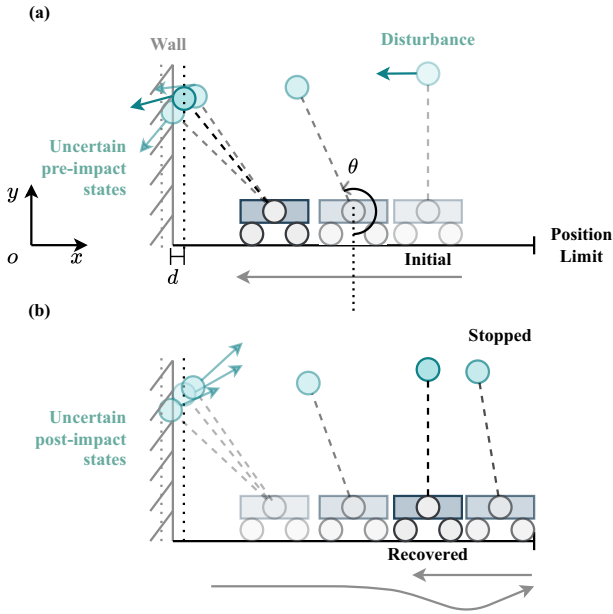


Fig. 7. Illustration of the cart-pole system recovering balance. (a) The pole angular velocity is disturbed. Since the cart input is limited, it moves to the wall to seek impact that will reverse the direction of pole velocity. (b) After Impact, the cart-pole can recover its balance and position.

can be written as

$$\mathbf{M}(\mathbf{q})\ddot{\mathbf{q}} + \mathbf{H}(\mathbf{q}, \dot{\mathbf{q}}) = [1, 0]^\top \tau + \mathbf{J}_c^\top \mathbf{F}_c \quad (15a)$$

$$\mathbf{M} = \begin{bmatrix} m_c + m_p & m_p l c_\theta \\ m_p l c_\theta & m_p l^2 \end{bmatrix}, \mathbf{H} = -m_p l s_\theta \begin{bmatrix} \dot{\theta}^2 \\ g \end{bmatrix}, \quad (15b)$$

where m_c, m_p are respectively the mass of the cart and the pole, l is the pole length (its CoM is assumed to be at the end), c_θ, s_θ are cosine and sine of the pole angle, τ is the cart linear driving force, $\mathbf{J}_c \in \mathbb{R}^{2 \times 2}$ is the contact jacobian of the pole and $\mathbf{F}_c \in \mathbb{R}^2$ is the wall reaction force. When the pole is upright, $\theta = \pi$. Its impact model is similar to (8) except that for the normal velocity w.r.t. the wall v_N , we assume a restitution coefficient C , such that

$$v_N^+ = -C v_N^-. \quad (16)$$

2) *Nominal Optimal Control*: The nominal optimal control comprises the pre-impact and post-impact phases. The pole is constrained to collide with the wall at the terminal node of the pre-impact phase. In the cases of early contact, the nominal optimal control is degraded into a single-phase problem with the post-impact states as its initial state. For late contact cases, the wall position is updated to the actual value if the nominal contact is not triggered.

3) *Proposed Method*: Since the cart-pole is an unstable and constrained system, it is important that the robot's state after the impact remains in a set from which there exists a solution to stabilize the system under the constraints (a.k.a viability). In general, finding this set is very difficult and out of the scope of this paper. Here, we present a simple brute-force approach to approximate this set. We used grid search to sample a small batch of pre-impact states $\mathbf{x} =$

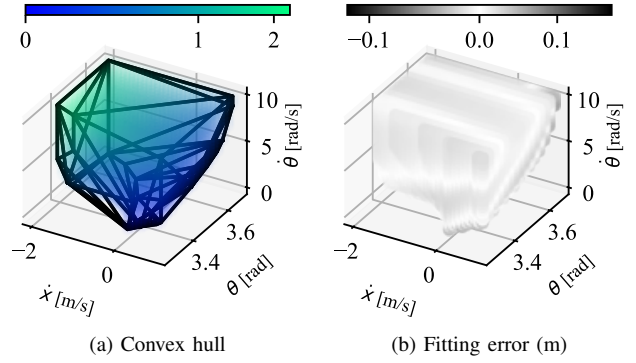


Fig. 8. Approximation of the feasible set of the cart-pole system. The colors represent (a) the stopping distance (unit: m) and (b) the fitting error of the quadratic approximation.

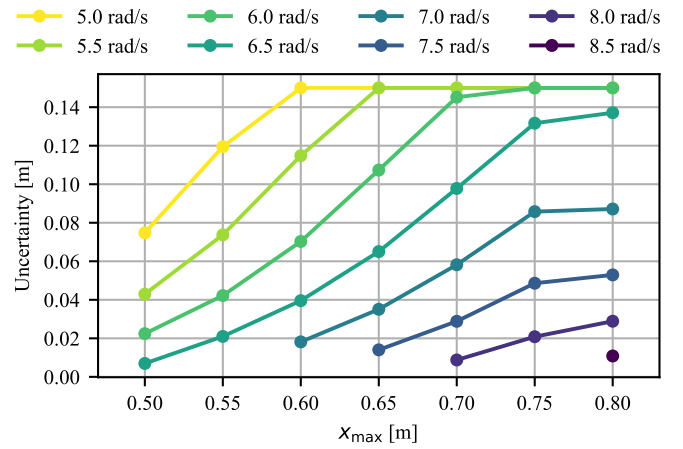


Fig. 9. Optimized uncertainty for difference disturbed angular velocities and position limits. Only feasible solutions are plotted.

$[\dot{x}, \theta, \dot{\theta}]^\top$ and approximated the feasible ones as a convex hull as shown in Fig. 8a. The stopping distance, i.e., the maximum position of the cart during the balancing, is approximated by a quadratic function ϕ of the pre-impact states as shown in Fig. 8b. These two approximations are sufficient for robust optimization with different x_{\max} .

Let $\mathbf{A}\mathbf{x} + \mathbf{b} \leq \mathbf{0}$ be the convex hull. The constraints of the robust phase can be designed as

$$\mathbf{h}_K^{\text{cvxh}} := \mathbf{A}\mathbf{x} + \mathbf{b} + \mathbf{s}, \quad (17a)$$

$$h_K^{\text{dist}} := \phi(\mathbf{x}) - x_{\max}, \quad (17b)$$

where \mathbf{s} is the conservativeness parameter, (17a) is the convex hull constraint and (17b) is the maximum stopping distance constraint.

Remark 3 (Conservativeness) Since the convex hull is merely an approximation of the feasible sample set, states close to its boundary may still be infeasible. The conservativeness parameters shrink the boundary to push the states into the interior to improve robustness.

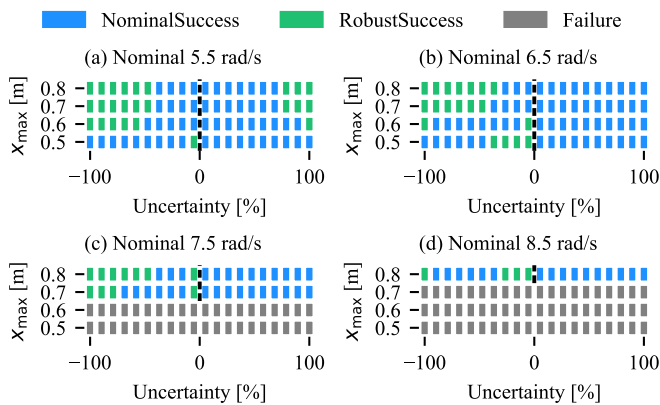


Fig. 10. Success-failure plot for the comparison experiment. ‘Nominal-Success’ denotes the success achieved by purely the nominal approach. ‘RobustSuccess’ denotes the success achieved by the robust method in addition to the ‘NominalSuccess’. Note that the robust method will also succeed in ‘NominalSuccess’ settings. The dashed lines denote that the nominal method can find a nominal solution for the given setting. Note that the blocks do not include the nominal settings (zero uncertainty).

4) *Results and Discussion:* The nominal and robust methods are tested on various $\dot{\theta}(0)$ and x_{\max} settings. The restitution coefficient in (16) is 0.8 and the friction coefficient is 0.7. The optimized uncertainties are shown in Fig. 9 where the monotonicity w.r.t. $\dot{\theta}(0)$ and x_{\max} can be summarized as respectively negative and positive.

The comparison results are shown in Fig. 10. The robust approach has a higher success rate for both early and late contact, while the nominal approach could fail. This phenomenon shows that the robustness of the nominal approach is limited by its potentially aggressive solution. Nevertheless, the robust approach cannot always ensure success since the feasibility of the original problem can vary between settings, which is irrelevant to uncertainty.

V. CONCLUSIONS AND FUTURE WORK

In this work, we present an uncertainty-aware optimal control formulation that takes the uncertainty in contact events into account using the notion of guards in hybrid systems and enables tractable resolution of the problem. Our proposed formulation features constraint satisfaction and uncertainty optimization within a robust phase, making it applicable to various problems in robotics with uncertain contact events. Several case studies showed that, in addition to generating robust trajectories, uncertainty optimization is important to avoid failure.

In the future, we plan to extend the uncertainty-aware approach to parallelized tree-structure optimal control for applications that emphasize long-term optimality. We also plan to implement a fast parameterized and constrained optimal control solver for real-world experiments. Real-world experiments are also part of our future vision for this work.

- [1] R. Deits and R. Tedrake, “Footstep planning on uneven terrain with mixed-integer convex optimization,” in *2014 IEEE-RAS international conference on humanoid robots*, pp. 279–286, IEEE, 2014.
- [2] M. A. Toussaint, K. R. Allen, K. A. Smith, and J. B. Tenenbaum, “Differentiable physics and stable modes for tool-use and manipulation planning,” 2018.
- [3] Y. Tassa, T. Erez, and E. Todorov, “Synthesis and stabilization of complex behaviors through online trajectory optimization,” in *2012 IEEE/RSJ International Conference on Intelligent Robots and Systems*, pp. 4906–4913, IEEE, 2012.
- [4] I. Mordatch, E. Todorov, and Z. Popović, “Discovery of complex behaviors through contact-invariant optimization,” *ACM Transactions on Graphics (ToG)*, vol. 31, no. 4, pp. 1–8, 2012.
- [5] M. Posa, C. Cantu, and R. Tedrake, “A direct method for trajectory optimization of rigid bodies through contact,” *The International Journal of Robotics Research*, vol. 33, no. 1, pp. 69–81, 2014.
- [6] M. Toussaint, J. Harris, J.-S. Ha, D. Driess, and W. Hönig, “Sequence-of-constraints mpc: Reactive timing-optimal control of sequential manipulation,” in *2022 IEEE/RSJ International Conference on Intelligent Robots and Systems (IROS)*, pp. 13753–13760, IEEE, 2022.
- [7] C. Mastalli, W. Merkt, G. Xin, J. Shim, M. Mistry, I. Havoutis, and S. Vijayakumar, “Agile maneuvers in legged robots: a predictive control approach,” *IEEE Transactions on Robotics*, 2023.
- [8] R. Grandia, F. Jenelten, S. Yang, F. Farshidian, and M. Hutter, “Perceptive locomotion through nonlinear model predictive control,” *IEEE Transactions on Robotics*, 2023.
- [9] A. Meduri, P. Shah, J. Viereck, M. Khadiv, I. Havoutis, and L. Righetti, “Biconmp: A nonlinear model predictive control framework for whole body motion planning,” *IEEE Transactions on Robotics*, 2023.
- [10] H. Zhu, A. Meduri, and L. Righetti, “Efficient object manipulation planning with monte carlo tree search,” in *2023 IEEE/RSJ international conference on intelligent robots and systems (IROS)*, IEEE, 2023.
- [11] L. Drnack and Y. Zhao, “Robust trajectory optimization over uncertain terrain with stochastic complementarity,” *IEEE Robotics and Automation Letters*, vol. 6, no. 2, pp. 1168–1175, 2021.
- [12] B. Hammoud, M. Khadiv, and L. Righetti, “Impedance optimization for uncertain contact interactions through risk sensitive optimal control,” *IEEE Robotics and Automation Letters*, vol. 6, no. 3, pp. 4766–4773, 2021.
- [13] A. Gazar, M. Khadiv, S. Kleff, A. Del Prete, and L. Righetti, “Nonlinear stochastic trajectory optimization for centroidal momentum motion generation of legged robots,” in *Robotics Research*, pp. 420–435, Springer Nature Switzerland Cham, 2023.
- [14] A. Gazar, M. Khadiv, A. Del Prete, and L. Righetti, “Multi-contact stochastic predictive control for legged robots with contact locations uncertainty,” *arXiv preprint arXiv:2309.04469*, 2023.
- [15] E. R. Westervelt, J. W. Grizzle, and D. E. Koditschek, “Hybrid zero dynamics of planar biped walkers,” *IEEE transactions on automatic control*, vol. 48, no. 1, pp. 42–56, 2003.
- [16] A. M. Johnson, S. A. Burden, and D. E. Koditschek, “A hybrid systems model for simple manipulation and self-manipulation systems,” *The International Journal of Robotics Research*, vol. 35, no. 11, pp. 1354–1392, 2016.
- [17] N. J. Kong, C. Li, G. Council, and A. M. Johnson, “Hybrid iLQR Model Predictive Control for Contact Implicit Stabilization on Legged Robots,” *IEEE Transactions on Robotics*, vol. 39, no. 6, pp. 4712–4727, 2023.
- [18] F. Farshidian *et al.*, “OCS2: An open source library for optimal control of switched systems.” [Online]. Available: <https://github.com/leggedrobotics/ocs2>.
- [19] C. Mastalli, R. Budhiraja, W. Merkt, G. Saurel, B. Hammoud, M. Naveau, J. Carpentier, L. Righetti, S. Vijayakumar, and N. Mansard, “Crocodyl: An Efficient and Versatile Framework for Multi-Contact Optimal Control,” in *2020 IEEE International Conference on Robotics and Automation (ICRA)*, pp. 2536–2542, 2020.
- [20] C. Mastalli, S. P. Chhatoi, T. Corbères, S. Tonneau, and S. Vijayakumar, “Inverse-dynamics mpc via nullspace resolution,” *IEEE Transactions on Robotics*, vol. 39, no. 4, pp. 3222–3241, 2023.
- [21] J. v. Steen, G. v. d. Brandt, N. v. d. Wouw, J. Kober, and A. Saccon, “Quadratic programming-based reference spreading control for dual-arm robotic manipulation with planned simultaneous impacts,” *IEEE Transactions on Robotics*, pp. 1–14, 2024.

- [22] A. Oshin, M. D. Houghton, M. J. Acheson, I. M. Gregory, and E. A. Theodorou, "Parameterized Differential Dynamic Programming," in *Robotics: Science and Systems 2022*, 2022.
- [23] G. Frison and M. Diehl, "HPIPM: a high-performance quadratic programming framework for model predictive control," *IFAC-PapersOnLine*, vol. 53, no. 2, pp. 6563–6569, 2020.
- [24] J. Andersson, J. Gillis, G. Horn, J. Rawlings, and M. Diehl, "CasADi: a software framework for nonlinear optimization and optimal control," *Mathematical Programming Computation*, vol. 11, 07 2018.
- [25] A. Wächter and L. T. Biegler, "On the implementation of an interior-point filter line-search algorithm for large-scale nonlinear programming," *Mathematical Programming*, vol. 106, pp. 25–57, 2006.
- [26] M. Bogdanovic, M. Khadiv, and L. Righetti, "Learning variable impedance control for contact sensitive tasks," *IEEE Robotics and Automation Letters*, vol. 5, no. 4, pp. 6129–6136, 2020.
- [27] A. Aydinoglu and M. Posa, "Real-time multi-contact model predictive control via admm," in *2022 IEEE/RAS International Conference on Robotics and Automation (ICRA)*, pp. 3414–3421, 05 2022.